Nonlinear modeling and control for an evaporator unit[1]

Christoph Josef Backi

Department of Chemical Engineering
Norwegian University of Science and Technology (NTNU)
N-7491 Trondheim

Email Address: christoph.backi@ntnu.no
Mobile: +47 944 79 561

Abstract

This article presents a nonlinear modeling approach describing the enthalpy dynamics between the inlet of the economizer and the outlet of the evaporator in a once-through boiler. The model is used to design an LQG controller for the steam quality at the evaporator outlet and to estimate the firing power, which constitutes a disturbance to the process. Robustness properties of the overall controller design are evaluated and the results are presented in simulations utilizing a high-fidelity model acting as the real plant.

Keywords: Once-Through Boiler, Power Plant Control, LQG, Kalman Filter, Disturbance Observer

1. Introduction

The control of steam parameters such as temperature and pressure or enthalpy in thermal power plants is crucial in order to ensure operation in a reliable and predictable way. This implies that only superheated steam not containing any liquid water is fed to the turbine units to avoid increased wear or damages to the turbines and increase efficiency. In addition, the steam parameters after the evaporator and before the superheater should be controlled to desired nominal, load-dependent values to guarantee smooth and predictable operation. This is achieved by controlling the feed water supply to the evaporator in accordance with load changes.

This work introduces a nonlinear dynamic modeling approach for the enthalpy dynamics between the inlet of the economizer and the outlet of the evaporator in thermal power plant, specifically in a

[1]Ideas for this work have been highlighted in [1], but have never been made publicly available due to a pending patent application by the Siemens AG, Munich, Germany resulting in the patent by [2]. A brief paper on the topic was published in [3].

once-through boiler. The model is utilized to design a dynamic controller for the feed water supply in order to operate the plant in a safe and reliable way. In addition, a state- and disturbance observer is designed based on the model to estimate the unmeasurable dynamic states and the heat power, whose deviations from a nominal, theoretic value constitute disturbances to the plant. This deviation might have many causes, such as fouling inside the evaporator leading to a decrease in heat transfer and varying heat value of the fuel. Disturbance observers have been applied to power plant related processes before, e.g. in [4] in the context of linear systems with PI control for a fluidized bed combustor.

The feed water supply can be controlled with PI controllers in a temperature-cascade, as for example described in [5]. The authors in [6] introduce an enthalpy state feedback controller for the superheating process in thermal power plants, which should replace the widely utilized temperature-cascade control. It is known that state regulators, compared to common PI controllers, in general deliver faster response times and a higher quality of control. Another reason for using enthalpy state control to replace temperature cascades can be found in the evaporation process itself, where it is specified that slightly superheated steam should be present at the end of the evaporator. This means that the evaporation endpoint is close to the saturated steam limit and hence, due to pressure changes, wet steam can be the consequence by regarding temperature as the controlled variable. In case of constantly controlled temperature, this ultimately causes the evaporation endpoint to change into the wet steam region of the p-h-diagram. On the other hand, explicitly considering pressure in the calculations becomes unnecessary when regarding enthalpy as state variable, since it inherently combines both temperature and pressure in one variable. Another advantage in considering enthalpies is pointed out in [6], namely that the system gain from inlet to outlet will be equal to one. This means that e.g. an enthalpy increase at the inlet will have the same stationary value at the outlet, whereas for temperatures this is not the case: A change in temperature at the inlet will lead to a different temperature change at the outlet, hence the gain is not equal to one.

In once-through boilers, the evaporating working fluid continuously flows through the boiler, meaning that the feed water pump supplies the feed water successively to the economizer, evaporator and superheater. In once-through boilers no drum is required inside the boiler since the feed water boils, evaporates and ultimately superheats in a continuous manner due to the supplied heat. In principle, there exist two different constructions for once-through boilers, the so called Sulzer and Benson types. The difference between these two lies in the operational mode; the Sulzer construction is designed for subcritical operation, meaning that the pressure typically lies below the critical point, whereas the

Benson type is often operated supercritically with pressures above the critical point. The present work focuses on Benson boilers, for which the works of e.g. [7], [8] and [9] provide more information as well as experience from suppliers and industry's sides.

Regarding the control of power plants in general, the work of [10] constitutes a rather old, yet not outdated piece of literature, which is still used by practitioners and beginners in the field. Novel ideas for a holistic view on boiler control are presented in [11]. Extensive work in recent years has led to the development of many modeling approaches for simulation studies and controller design. [12] present a simulation study using the software *gPROMS* with a simple model for a subcritical power plant, concluding that their model, validated against real data, showed relative errors < 5 % for as low as 70 % load. Dynamic modeling approaches for ultra-supercritical coal fired once-through boiler-turbine units are introduced by [13, 14]. The authors in [13] conclude that their model matches well with operational data in steady-state as well as in transients and hence complexity reduction for controller design is viable. In [14] a genetic algorithm is used to identify parameters of the plant with the conclusion that the procedure leads to a model that delivers good results when validated with real plant data, both open- and closed-loop. A general, control-oriented modeling approach for a boiler-turbine unit with rather simple models, utilizing PI controllers and parameter identification is proposed in [15]. The authors conclude that the accuracy of the model was confirmed by field measurements. Modeling strategies based on distributed parameter systems together with simulation studies for large coal-fired power plants are presented in [16, 17]. A dynamic model of a natural water circulation boiler for on-line monitoring of fuels is introduced in [18].

The remainder of this paper is structured as follows: In Section 2 the mathematical model is derived and presented, whereas Section 3 introduces the design of the controller and observer as well as a robustness analysis for the closed-loop system. Section 4 shows simulation results for different cases regarding load changes, disturbances, noise and specific uncertainties utilizing a high-fidelity model of the real plant. The results are discussed and the paper is concluded in Section 5.

2. Mathematical Model

As mentioned in the Introduction, the model that has been developed describes the enthalpy dynamics between the inlet of the economizer and the outlet of the evaporator. In the economizer, the unused heat of the flue gas is exploited to pre-warm the feed water before it enters the boiler unit. The feed water then enters the evaporator, where it evaporates and at whose outlet the steam parameters should be located just outside the wet steam region in the p-h-diagram, hence dry steam should be available before entering the superheating stages. A schematic of the considered parts in the power plant process is presented in Figure 1.

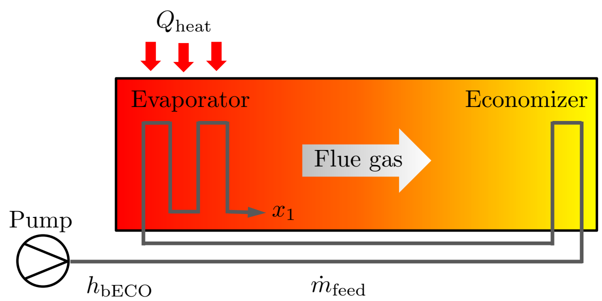

Figure 1: Schematic of the considered parts in the power plant process

The authors in [6] and [19] argue that for a superheater unit, the input-output-dynamics can be modeled by high-order lags. The same principle can be used to model the input-output-dynamics of the evaporator unit. The order of such a model is not explicitly stated, however, from experience and observations it can be inferred that these can be approximated by a third-order lag. Nevertheless, a comparison of dynamic (step-)responses for higher order lags, e.g. of order 3 up to 6, indicates that there is no significant difference between the single high-order lags, presumed that the overall time constant is not changing. Hence, not the order of the dynamics, but the difference in time constants between the plant and the model is of high importance for the plant-model-mismatch and ultimately for robustness. This topic is addressed in Section 3.5 by a robustness analysis with respect to differences in time constants. Nevertheless, an investigation of the dynamic behavior of the controller will be conducted, where a model of higher order acts as the real plant; the plant model has thereby order six, whereas the controller model is formulated as a third-order model. In general, accurate identification of the dynamics is a difficult task since it is affected by many factors such as the degree of fouling inside the boiler unit and the operating point. Furthermore, the pursued robust nature of the controller makes a precise modeling of the dynamics unnecessary. The nature of the process dictates thereby that the time constant of the model depends on the load, which means that with increasing load the time constant becomes smaller, and vice versa. Thus, the third-order model can be stated as follows

$$
\begin{aligned}
\dot{x}_1 &= \frac{1}{\dot{m}_{\text{feed,full}}\, T_{\text{full}}} \left(\frac{Q_{\text{heat}}}{3} + \dot{m}_{\text{feed}}(x_2 - x_1) \right), \\
\dot{x}_2 &= \frac{1}{\dot{m}_{\text{feed,full}}\, T_{\text{full}}} \left(\frac{Q_{\text{heat}}}{3} + \dot{m}_{\text{feed}}(x_3 - x_2) \right), \\
\dot{x}_3 &= \frac{1}{\dot{m}_{\text{feed,full}}\, T_{\text{full}}} \left(\frac{Q_{\text{heat}}}{3} + \dot{m}_{\text{feed}}(h_{\text{bECO}} - x_3) \right), \\
y &= x_1,
\end{aligned}
\tag{1}
$$

where $\dot{m}_{\text{feed}} = u$ denotes the input (manipulated variable), which is the feed water mass flow. Furthermore, x_1 is the enthalpy after evaporator h_{bECO} is the enthalpy before economizer, x_2 and x_3 are enthalpies between h_{bECO} and x_1, and Q_{heat} indicates the supplied heat power. Latter can be calculated via

$$Q_{\text{heat}} = \eta \dot{m}_{\text{fuel}} H_{\text{u}},$$

where η is an empirical, load-dependent efficiency factor, $\dot{m}_{\text{fuel}}$ represents the mass flow of fuel and H_{u} indicates the heat value of the fuel. The index 'full' labels constant scaling parameters at full load, where the effective, load-dependent time constant of the system can be calculated via

$$T_{\text{sys}} = T_{\text{full}} \frac{\dot{m}_{\text{feed,full}}}{\dot{m}_{\text{feed}}}.$$

The enthalpy after evaporator (state x_1) is the measured variable (output) of the system.

It is pointed out that the pressure dynamics are not explicitly included in this modeling approach, since these are much faster compared to those of heat exchange. Hence, a load-independent and constant pressure-drop between the inlet of the economizer and the outlet of the evaporator is assumed.

2.1. Linearization

The design of LQG controllers–an Extended Kalman Filter (EKF) in combination with a Linear Quadratic Regulator (LQR)–requires the system dynamics (1) to be linearized. This can be achieved by defining the respective steady states for x_1, x_2 and x_3, which can be found by setting the time-derivatives in (1) to zero

$$
\begin{aligned}
x_{3,0} &= \frac{Q_{\text{heat}}}{3\,\dot{m}_{\text{feed}}} + h_{\text{bECO}},\\
x_{2,0} &= \frac{Q_{\text{heat}}}{3\,\dot{m}_{\text{feed}}} + x_{3,0} = \frac{2\,Q_{\text{heat}}}{3\,\dot{m}_{\text{feed}}} + h_{\text{bECO}},\\
x_{1,0} &= \frac{Q_{\text{heat}}}{3\,\dot{m}_{\text{feed}}} + x_{2,0} = \frac{Q_{\text{heat}}}{\dot{m}_{\text{feed}}} + h_{\text{bECO}},
\end{aligned}
$$

where the stationary value $x_{1,0}$ defines the desired enthalpy after evaporator $x_{1,\text{d}} = h_{\text{d}}$. With this information, the required feed water mass flow $\dot{m}_{\text{req}}$ can be calculated as

$$
\dot{m}_{\text{req}} = \frac{Q_{\text{heat}}}{h_{\text{d}} - h_{\text{bECO}}}. \tag{2}
$$

The remaining two desired steady states $x_{2,0} = x_{2,\text{d}}$ and $x_{3,0} = x_{3,\text{d}}$ can be defined as functions of h_{bECO} and h_{d}

$$
\begin{aligned}
x_{2,\text{d}} &= \frac{2\,h_{\text{d}} + h_{\text{bECO}}}{3},\\
x_{3,\text{d}} &= \frac{h_{\text{d}} + 2\,h_{\text{bECO}}}{3}.
\end{aligned} \tag{3}
$$

Following the principle of linearization of dynamic systems, the original states x_i can be expressed as a sum of the steady / desired state values and small perturbations around these setpoints, for which the linearization is valid

$$
\begin{aligned}
x_1 &= h_{\text{d}} + \Delta x_1 \Rightarrow \dot{x}_1 = \Delta \dot{x}_1,\\
x_2 &= x_{2,\text{d}} + \Delta x_2 \Rightarrow \dot{x}_2 = \Delta \dot{x}_2,\\
x_3 &= x_{3,\text{d}} + \Delta x_3 \Rightarrow \dot{x}_3 = \Delta \dot{x}_3,\\
u &= \dot{m}_{\text{req}} + \Delta u.
\end{aligned}
$$

After putting these equations into (1), and assuming that all multiplications of perturbations are small and can be set to zero, one obtains

$$
\begin{aligned}
\Delta\dot{x}_1 &= G\left(\frac{Q_{\text{heat}}}{h_{\text{d}}-h_{\text{bECO}}}(\Delta x_2-\Delta x_1)-\frac{h_{\text{d}}-h_{\text{bECO}}}{3}\Delta u\right),\\
\Delta\dot{x}_2 &= G\left(\frac{Q_{\text{heat}}}{h_{\text{d}}-h_{\text{bECO}}}(\Delta x_3-\Delta x_2)-\frac{h_{\text{d}}-h_{\text{bECO}}}{3}\Delta u\right),\\
\Delta\dot{x}_3 &= G\left(-\frac{Q_{\text{heat}}}{h_{\text{d}}-h_{\text{bECO}}}\Delta x_3-\frac{h_{\text{d}}-h_{\text{bECO}}}{3}\Delta u\right),\\
y &= h_{\text{d}}+\Delta x_1,
\end{aligned}
\tag{4}
$$

with $G = \dfrac{1}{\dot{m}_{\text{feed,full}}\,T_{\text{full}}}$ leading to the state space form

$$
\begin{aligned}
\Delta\dot{\mathbf{x}} &= \mathbf{A}\Delta\mathbf{x}+\mathbf{B}\Delta u,\\
y &= \mathbf{C}\Delta\mathbf{x}+h_{\text{d}},
\end{aligned}
$$

where

$$
\mathbf{A} = G\frac{Q_{\text{heat}}}{(h_{\text{d}}-h_{\text{bECO}})}\begin{bmatrix}-1 & 1 & 0\\ 0 & -1 & 1\\ 0 & 0 & -1\end{bmatrix},\quad \mathbf{B} = \frac{G}{3}(h_{\text{d}}-h_{\text{bECO}})\begin{bmatrix}-1\\-1\\-1\end{bmatrix},\quad \mathbf{C} = \begin{bmatrix}1 & 0 & 0\end{bmatrix}.
$$

The system matrix $\mathbf{A}$ and the input matrix $\mathbf{B}$ are load-dependent since they include the desired enthalpy after evaporator h_{d}. This means that the dynamics are updated over the whole load range and adapted to the present load. However, the linearized dynamics (4) only hold for small deviations around the defined steady / desired states $x_{1,\text{d}}$, $x_{2,\text{d}}$ and $x_{3,\text{d}}$.

3. Controller and observer design

This Section presents a combined (optimal) controller and observer design for the feed water supply, state- and disturbance estimation.

Figure 2 pictures the overall structure with the *Plant*, *Actuation Dynamics* for the feed water supply (a first-order lag), the *LQG Controller* and a *Pre-Calculation* block. The latter two are shown in Figures 3 and 4, respectively.

In Figure 3 the *Pre-Calculation* block is presented. The respective *Lookup Tables* represent linear interpolations between certain load points (see Appendix). The pressure dynamics are delayed by

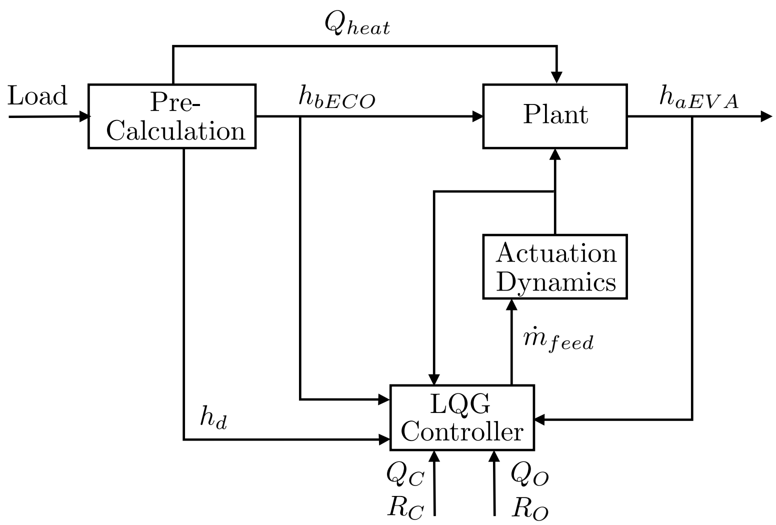

Figure 2: Structure of the overall system; the index 'aEVA' denotes 'after evaporator'

third-order lags (denoted PT_3), whereas the efficiency factor η and the mass flow of fuel $\dot{m}_{\mathrm{fuel}}$ are delayed by first-order lags (denoted PT_1). The pressure p_{bECO} and the temperature before economizer $\vartheta_{\mathrm{bECO}}$ are fed into a *Water-Steam-Table* to calculate the enthalpy h_{bECO}.

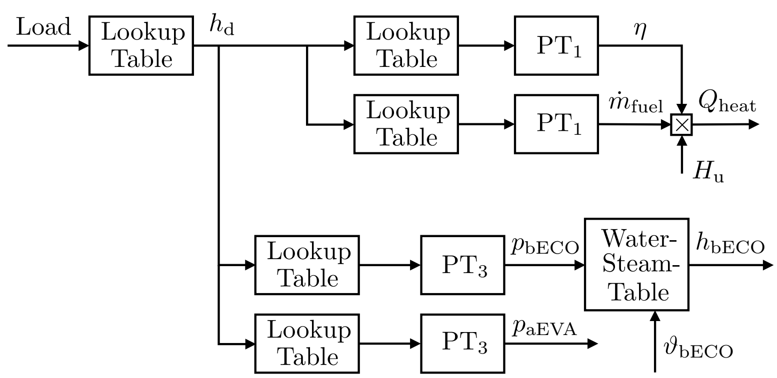

Figure 3: The Pre-Calculation providing load-dependent values to the *Plant* and the *LQG Controller*

3.1. LQ Regulator

The LQ Regulator (LQR) is an optimal state feedback control law based upon full state feedback. This implies that unmeasurable states must be estimated, which requires full observability of the system, or that unobservable states are stable, commonly known as detectability.

It must be pointed out that the LQR presented in this application is not of standard type. Just like a continuous Kalman Filter it is based on forward integration, which has been presented in e.g. [20] and [21]. This implies that the calculation of the state-feedback gain is adaptive with respect to changes in the system dynamics and minimizes the quadratic cost function

$$J = \int_{t_0}^{t_f} \left(\mathbf{x}^T(t)\mathbf{Q_C}\mathbf{x}(t) + u^T(t)R_C u(t) \right) dt, \tag{5}$$

where here $\mathbf{Q_C} = \begin{bmatrix} q_{C,1} & 0 & 0 \\ 0 & q_{C,2} & 0 \\ 0 & 0 & q_{C,3} \end{bmatrix}$ and R_C is a scalar.

In (5), the cross term $2\mathbf{x}^T\mathbf{N}u$ between states and input is neglected, meaning that $\mathbf{N} = \begin{bmatrix} 0 & 0 & 0 \end{bmatrix}^T$.

The state feedback law has the standard form

$$\Delta u = \mathbf{K}(t)_{(1\times3)} \begin{bmatrix} \hat{x}_1 - h_d \\ \hat{x}_2 - x_{2,\mathrm{d}} \\ \hat{x}_3 - x_{3,\mathrm{d}} \end{bmatrix},$$

where the feedback states are the estimated states and the feedback gain $\mathbf{K}(t)$ is calculated by solving the following differential Matrix-Riccati-Equations

$$\begin{aligned} \frac{d\mathbf{S}(t)}{dt} &= \mathbf{A}^T(t)\mathbf{S}(t) + \mathbf{S}(t)\mathbf{A}(t) - \mathbf{S}(t)\mathbf{B}(t)R_C^{-1}\mathbf{B}^T(t)\mathbf{S}(t) + \mathbf{Q_C}, \\ \mathbf{K}(t) &= R_C^{-1}\mathbf{B}^T(t)\mathbf{S}(t). \end{aligned} \tag{6}$$

There exist some requirements for the LQR to be implementable, namely

C.1) $(\mathbf{A}, \mathbf{B})$ stabilizable (all unstable modes are controllable)

C.2) $\tilde{\mathbf{Q}}_\mathbf{C} = \mathbf{Q_C} - \mathbf{N}R^{-1}\mathbf{N}^T$ positively semi-definite

C.3) R_C positively definite

C.4) $(\tilde{\mathbf{Q}}_\mathbf{C}, \mathbf{A} - \mathbf{B}R^{-1}\mathbf{N}^T)$ detectable

The standard controllability matrix $\begin{bmatrix} \mathbf{B} & \mathbf{AB} & \mathbf{A}^2\mathbf{B} \end{bmatrix}$ in point C.1) has full rank, except for the case if $h_\mathrm{d} \equiv h_\mathrm{bECO}$ (or $Q_\mathrm{heat} \equiv 0$), for which the model is not designed and which is never the case in regular operation. Points C.2)–C.3) are degrees of freedom, which can be fulfilled by the right choice of the respective matrices. Since $\mathbf{N} = \begin{bmatrix} 0 & 0 & 0 \end{bmatrix}^T$, the matrix $\begin{bmatrix} \mathbf{Q_C} & \mathbf{Q_C A} & \mathbf{Q_C A}^2 \end{bmatrix}^T$ in point C.4) has full rank except for the case if $q_{C,1} \equiv 0$, which can be chosen accordingly. Hence, the LQR can be implemented.

Remark 1. *It must be mentioned that any other state feedback control law could be implemented here, e.g. utilizing a static feedback gain. The choice to implement the method described above is justified by the supposedly improved performance of state feedback with varying gains. Therefore, the state feedback control law presented above depicts merely one option and should be subject to a deeper investigation before being applied to a real plant. This holds especially in the context of stability, which, however, is not the scope of this work. Nonetheless, the state feedback in the system at hand only has a small share in the overall control action, since the main portion is provided by the feedforward part, see* (2)*.*

3.2. Augmented Extended Kalman Filter as state and disturbance observer

As mentioned earlier, full state feedback controllers can only be implemented if all states are available for feedback. This means that unmeasurable states must be estimated, which requires full observability of the plant model. It will be shown that all states of the plant model can be estimated by the Extended Kalman Filter, which is a robust (and optimal) estimation algorithm. Additionally, an estimate for a disturbance variable, namely the uncertain heat power Q_{heat}, will be introduced by augmenting the states in the EKF.

Hence, the same dynamics as already introduced in (1) are considered, but augmented by an additional fourth state $\hat{x}_4$ representing the estimated heat power $\hat{Q}_{\text{heat}}$. Its dynamics are thereby added in a quasi-stationary fashion. In addition, the respective observer output feedback laws $L_i(t)(h_{\text{aEVA,m}} - \hat{y})$ are added to the respective state derivatives $\dot{\hat{x}}_i$ resulting in the dynamic equations for the EKF

$$
\begin{aligned}
\dot{\hat{x}}_1 =& G_O\left(\frac{\hat{x}_4}{3} + \dot{m}_{\text{feed}}(\hat{x}_2 - \hat{x}_1)\right) + L_1(t)(h_{\text{aEVA,m}} - \hat{y}),\\
\dot{\hat{x}}_2 =& G_O\left(\frac{\hat{x}_4}{3} + \dot{m}_{\text{feed}}(\hat{x}_3 - \hat{x}_2)\right) + L_2(t)(h_{\text{aEVA,m}} - \hat{y}),\\
\dot{\hat{x}}_3 =& G_O\left(\frac{\hat{x}_4}{3} + \dot{m}_{\text{feed}}(h_{\text{bECO}} - \hat{x}_3)\right) + L_3(t)(h_{\text{aEVA,m}} - \hat{y}),\\
\dot{\hat{x}}_4 =& L_4(t)(h_{\text{aEVA,m}} - \hat{y}),\\
\hat{y} =& \hat{x}_1,
\end{aligned}
\tag{7}
$$

where $G_O = \dfrac{1}{\dot{m}_{\text{feed,full}}\, T_{\text{full,O}}}$, $T_{\text{full,O}}$ is the time constant chosen in the LQG controller and $h_{\text{aEVA,m}}$ denotes the measured enthalpy after evaporator.

The set of equations (7) can be rewritten in state-space form as

$$
\begin{aligned}
\Delta\dot{\hat{\mathbf{x}}} &= \mathbf{A_O}\Delta\hat{\mathbf{x}} + \mathbf{B_O}\Delta u + \mathbf{L}(t)(h_{\text{aEVA,m}} - \hat{y}),\\
\Delta y &= \mathbf{C_O}\Delta\hat{\mathbf{x}} + h_{\text{d}},
\end{aligned}
$$

where

$$
\mathbf{A_O} = G_O\begin{bmatrix} -\dot{\hat{m}}_{\text{req}} & \dot{\hat{m}}_{\text{req}} & 0 & \frac{1}{3}\\ 0 & -\dot{\hat{m}}_{\text{req}} & \dot{\hat{m}}_{\text{req}} & \frac{1}{3}\\ 0 & 0 & -\dot{\hat{m}}_{\text{req}} & \frac{1}{3}\\ 0 & 0 & 0 & 0 \end{bmatrix}, \quad \mathbf{B_O} = \frac{G_O}{3}(h_{\text{d}} - h_{\text{bECO}})\begin{bmatrix} -1\\ -1\\ -1\\ 0 \end{bmatrix}, \quad \mathbf{C_O} = \begin{bmatrix} 1 & 0 & 0 & 0 \end{bmatrix},
$$

with $\dot{\hat{m}}_{\text{req}} = \dfrac{\hat{x}_4}{h_{\text{d}} + h_{\text{bECO}}}$ according to (2).

The time-varying Kalman feedback gain $\mathbf{L}(t)$ is calculated with the following differential Matrix-Riccati-Equations

$$
\begin{aligned}
\frac{d\mathbf{P}(t)}{dt} &= \mathbf{A_O}(t)\mathbf{P}(t) + \mathbf{P}(t)\mathbf{A_O}^T(t) - \mathbf{P}(t)\mathbf{C_O}^T(t)R_O^{-1}\mathbf{C_O}(t)\mathbf{P}(t) + \mathbf{Q_O},\\
\mathbf{L}(t) &= \mathbf{P}(t)\mathbf{C_O}^T(t)R_O^{-1},
\end{aligned}
\tag{8}
$$

where $\mathbf{Q_O} = \text{cov}\{\mathbf{w}(t)\mathbf{w}^T(t)\} = \begin{bmatrix} q_{O,1} & 0 & 0 & 0 \\ 0 & q_{O,2} & 0 & 0 \\ 0 & 0 & q_{O,3} & 0 \\ 0 & 0 & 0 & q_{O,4} \end{bmatrix}$ denotes the covariance of the process noise $\mathbf{w}(t)$ and $R_O = \text{cov}\{v(t)v^T(t)\}$ defines the covariance of the measurement noise $v(t)$. No covariance is assumed between the two noises, hence $\mathbf{W_O} = \text{cov}\{\mathbf{w}(t)v^T(t)\} = \begin{bmatrix} 0 & 0 & 0 \end{bmatrix}^T$. It is assumed that the noises enter the plant in the following way

$$\dot{\mathbf{x}} = \mathbf{A_O}\mathbf{x} + \mathbf{B_O}u + \mathbf{\Gamma}\mathbf{w}(t),$$
$$y = \mathbf{C_O}\mathbf{x} + \mathbf{\Lambda}\mathbf{w}(t) + v(t),$$

with $\mathbf{\Gamma} = \mathbf{I}_3$ (identity matrix of size 3) and $\mathbf{\Lambda} = \begin{bmatrix} 0 & 0 & 0 \end{bmatrix}$.

Just like for the LQR, some requirements must also be fulfilled for the EKF to be implementable:

O.1) $(\mathbf{C_O}, \mathbf{A_O})$ detectable (all unstable modes are observable)

O.2) $\tilde{R}_O = R_O + \mathbf{\Lambda}\mathbf{W_O} + \mathbf{W_O}^T\mathbf{\Lambda}^T + \mathbf{\Lambda}\mathbf{Q_O}\mathbf{\Lambda}^T$ positively definite

O.3) $\tilde{\mathbf{Q}}_\mathbf{O} = \mathbf{\Gamma}\mathbf{Q_O}\mathbf{\Gamma}^T - \tilde{\mathbf{W}}_\mathbf{O}\tilde{R}_O^{-1}\tilde{\mathbf{W}}_\mathbf{O}^T$ positively semi-definite

O.4) $(\mathbf{A_O} - \tilde{\mathbf{W}}_\mathbf{O}\tilde{R}_O^{-1}\mathbf{C_O}, \tilde{\mathbf{Q}}_\mathbf{O})$ stabilizable

with $\tilde{\mathbf{W}}_\mathbf{O} = \mathbf{\Gamma}\left(\mathbf{Q_O}\mathbf{\Lambda}^T + \mathbf{W_O}\right)$.

The requirements for the observer are fulfilled by the right choice of the matrix $\mathbf{Q_O}$ and the scalar R_O, respectively. In fact, the standard observability matrix $\begin{bmatrix} \mathbf{C_O} & \mathbf{C_O}\mathbf{A_O} & \mathbf{C_O}\mathbf{A_O}^2 & \mathbf{C_O}\mathbf{A_O}^3 \end{bmatrix}^T$ in point O.1) above has full rank, except for the case if $\dot{\hat{m}}_{\text{req}} \equiv 0$. Points O.2)–O.3) are degrees of freedom. The choice of $\mathbf{W_O} = \begin{bmatrix} 0 & 0 & 0 \end{bmatrix}^T$ leads to $\tilde{\mathbf{Q}}_\mathbf{O} \equiv \mathbf{Q_O}$ in point O.3). Thus, the controllability matrix in point O.4) simplifies to $\begin{bmatrix} \mathbf{Q_O} & \mathbf{A_O}\mathbf{Q_O} & \mathbf{A_O}^2\mathbf{Q_O} & \mathbf{A_O}^3\mathbf{Q_O} \end{bmatrix}$ and has full rank except for $q_{O,4} \equiv 0$, which can be chosen appropriately.

3.3. Alternative formulation of the differential Matrix-Riccati-Equation

In order to simplify the tuning procedure for the Extended Kalman Filter in Section 3.2, the differential Matrix-Riccati-Equation (8) can be reformulated

$$\begin{aligned} \frac{d\mathbf{P}(t)}{dt} &= \mathbf{A_O}\mathbf{P}(t) + \mathbf{P}(t)\mathbf{A_O}^T - \alpha\mathbf{P}(t)\mathbf{C_O}^T R_O^{-1}\mathbf{C_O}\mathbf{P}(t) + \alpha\mathbf{P}(t), \\ \mathbf{L}(t) &= \alpha\mathbf{P}(t)\mathbf{C_O}^T R_O^{-1}, \end{aligned} \tag{9}$$

where α is a scalar forgetting factor. This observer design is known as a Kalman-like least-squares observer (KF-like LSO) with forgetting factor first introduced in [22] and further developed in [23] and [24]. The advantage in using (9) instead of (8) can be found in the simpler tuning procedure, at least for multivariable systems. As can be seen, (9) does not depend on the process noise covariance matrix $\mathbf{Q_O}$ and hence tuning is solely achieved by defining the measurement covariance matrix R_O and the scalar α. $\mathbf{Q_O}$ is often not known anyhow and in many cases offers too many degrees of freedom, particularly for multivariable systems. Thus, applying a Kalman-Filter with a differential Matrix-Riccati-Equation as in (9) offers a good alternative to the standard (Extended) Kalman Filter in Section 3.2.

3.4. LQG controller

A schematic of the LQG controller is displayed in Figure 4, where the block *Desired State Calculation* is based on (3), the blocks *Solver Riccati Controller* and *Solver Riccati Observer* are established by (6) and (8) or (9), respectively. The block *Nonlinear Model* is based on (7), where $\dot{m}_{\mathrm{feed}}$ labels the delayed feed water supply to the plant due to actuation dynamics modeled as first-order lags (see Figure 2) and $h_{\mathrm{aEVA,m}}$ is the measured enthalpy after evaporator.

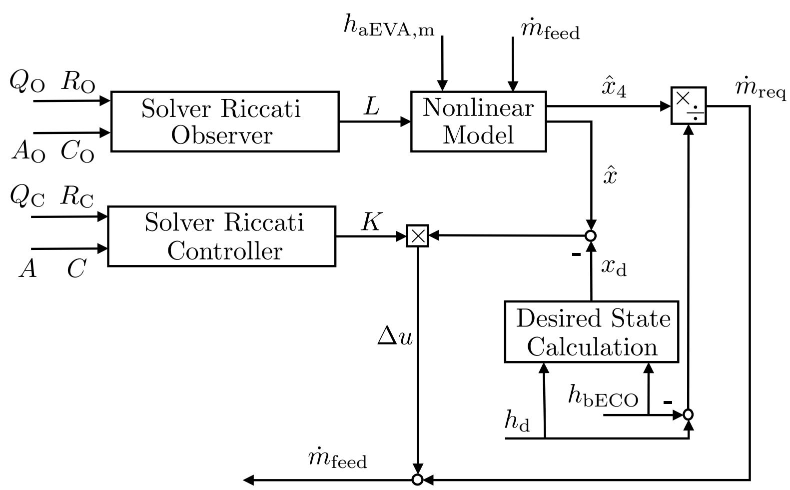

Figure 4: Schematic of the LQG controller

3.5. Robustness

An essential uncertainty between the model and a real plant is the difference between the two time constants T_{full} and $T_{\mathrm{full,O}}$. Therefore, a robustness analysis is performed, which investigates the damping ratio of the linear closed loop dynamics:

$$\begin{bmatrix} \dot{\mathbf{x}} \\ \dot{\hat{\mathbf{x}}} \end{bmatrix} = \begin{bmatrix} [\mathbf{A}] & \left[\mathbf{B}\left[-\mathbf{K}^T \dfrac{1}{h_\mathrm{d} - h_\mathrm{bECO}}\right]\right] \\ [\mathbf{LC}] & \left[\mathbf{A_O} - \mathbf{LC_O} + \mathbf{B_O}\left[-\mathbf{K}^T \dfrac{1}{h_\mathrm{d} - h_\mathrm{bECO}}\right]\right] \end{bmatrix} \begin{bmatrix} \mathbf{x} \\ \hat{\mathbf{x}} \end{bmatrix}$$

Thereby, for each (complex) eigenvalue λ_i a realistic value for the damping ratio $d_i = \frac{\mathrm{Re}(\lambda_i)}{|\lambda_i|}$ is chosen to be greater than 0.3. It must be mentioned that the investigation was conducted for constant, optimal feedback gains $\mathbf{L}$ and $\mathbf{K}$, respectively. However, in order to regard for dynamic behavior, the feed water mass flow was changed over a large operational range, in addition. The investigation is presented in the Simulations-Section 5.2.

As an additional indicator of the robustness properties of the controller, especially with respect to plant-model-mismatch, the dynamics of the plant are changed to sixth-order dynamics and simulation studies are conducted for this case, see Section 5.1. Thereby, the plant takes the shape

$$\begin{aligned} \dot{x}_1 &= \frac{1}{\dot{m}_\mathrm{feed,full}\, T_\mathrm{full}} \left(\frac{Q_\mathrm{heat}}{6} + \dot{m}_\mathrm{feed}(x_2 - x_1) \right), \\ \dot{x}_2 &= \frac{1}{\dot{m}_\mathrm{feed,full}\, T_\mathrm{full}} \left(\frac{Q_\mathrm{heat}}{6} + \dot{m}_\mathrm{feed}(x_3 - x_2) \right), \\ &\vdots \\ \dot{x}_6 &= \frac{1}{\dot{m}_\mathrm{feed,full}\, T_\mathrm{full}} \left(\frac{Q_\mathrm{heat}}{6} + \dot{m}_\mathrm{feed}(h_\mathrm{bECO} - x_6) \right), \end{aligned} \tag{10}$$

with steady states (the steady state feed water mass flow remains the same as in (2))

$$\begin{aligned} x_{1,\mathrm{d}} &= h_d, & x_{2,\mathrm{d}} &= \frac{5\ h_\mathrm{d} + h_\mathrm{bECO}}{6}, & x_{3,\mathrm{d}} &= \frac{2\ h_\mathrm{d} + h_\mathrm{bECO}}{3}, \\ x_{4,\mathrm{d}} &= \frac{h_\mathrm{d} + h_\mathrm{bECO}}{2}, & x_{5,\mathrm{d}} &= \frac{h_\mathrm{d} + 2\ h_\mathrm{bECO}}{3}, & x_{6,\mathrm{d}} &= \frac{h_\mathrm{d} + 5\ h_\mathrm{bECO}}{6}. \end{aligned} \tag{11}$$

Comparing the steady states in (3) and (11), it can be seen that the steady states $x_{3,\mathrm{d}}$ and $x_{5,\mathrm{d}}$ for the sixth order system (11) correspond with $x_{2,\mathrm{d}}$ and $x_{3,\mathrm{d}}$ for the third order system (3), respectively. Hence, the states x_3 and x_5 in (10) correspond with x_2 and x_3 in (1) and thus x_3 can be compared to $\hat{x}_2$ and x_5 to $\hat{x}_3$ regarding observer performance.

4. Simulation Results

In this Section, simulation results for different cases regarding load changes as well as the handling of disturbances, noise and parameter uncertainties are highlighted demonstrating the performance and robust nature of the LQG controller. The simulation and tuning parameters are listed in the Appendix.

4.1. Load change by two consecutive ramps

The simulation example in Figure 5 shows a load change from initially 35 % to 70 % and finally to 100 %. The load changes are applied with a slope of 1 % per 100 s. The LQG controller's time constant is fixed at $T_{\mathrm{full,O}} = 40$ s, whereas the plant's time constant T_{full} changes with the current load, which can be seen in the plot on the bottom right. The difference in time constants lead to a significant uncertainty and difference in the dynamical responses of the plant and the observer, respectively. In order to show the performance of the LQG controller under steady load changes and diverging time constants, no additive noise was applied to the plant. The overall performance of estimation is good and improves as T_{full} approaches $T_{\mathrm{full,O}}$ (for $t_{\mathrm{sim}} \to t_{\mathrm{end}}$). This is depicted in the individual state(-error) plots and the plot of the feed water mass flow.

4.2. Noisy measurement of $h_{\mathrm{aEVA,m}}$, disturbance in Q_{heat} and process noise

This section presents simulation results for 100 % load, where noise is not only added to the measurement $y = x_1$, but also to the process itself (process noise). Additionally, the estimation of the disturbance variable is demonstrated by adding a theoretical and rather large fluctuation in the provided heat power $\Delta Q_{\mathrm{heat}} = 100$ MW at $t = 100$ s. The respective time constant of the LQG controller is chosen to be $T_{\mathrm{full,O}} = 40$ s, whereas that of the plant is set to $T_{\mathrm{full}} = \{40, 80\}$ s. Performances of the two observer designs in Sections 3.2 and 3.3 are compared in addition. Figure 6 shows the results for the EKF design, whereas Figure 7 depicts those obtained by the KF-like LSO. In all Figures, the three top plots depict the state variables x_i together with their respective estimates $\hat{x}_i$, $i = 1, \ldots, 3$. The two plots on the bottom show the feed water mass flow as well as the estimated and nominal value of the provided heat power, respectively. Despite the very large, theoretical step change in the heat power, the states and the feed water mass flow are set to their (new) nominal values by the controller. Comparing the performance of the EKF and the KF-like LSO, it is apparent that the latter has better performance with respect to noise suppression. This, however, has the cost of slower convergence rates and larger overshoots for the state variables.

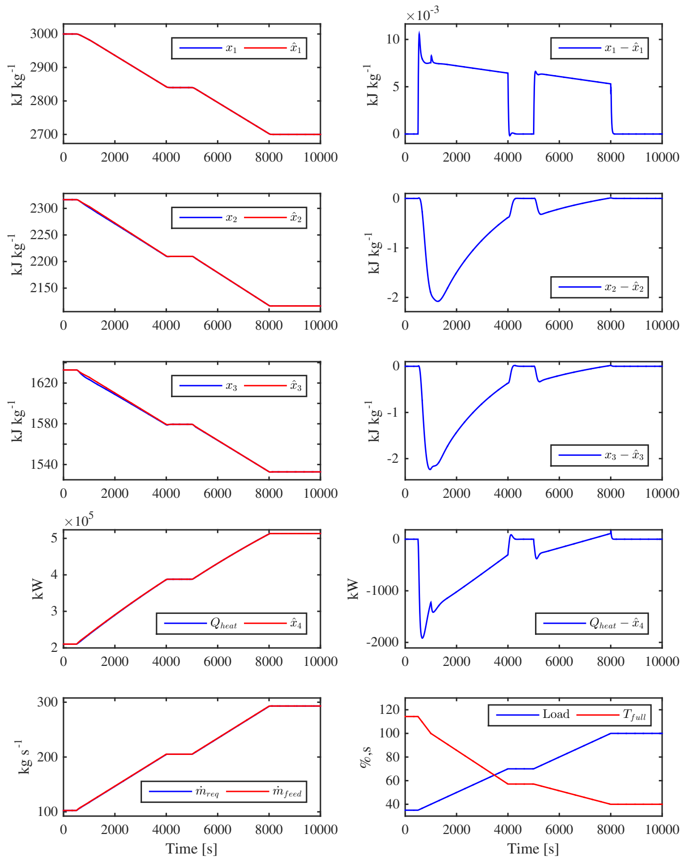

Figure 5: Performance of the closed loop system subject to ramp changes of the load from 35 % to 70 % and 100 %

4.3. Disturbance in h_{bECO}

Now, a simulation study at 100 % load is demonstrated in Figure 8 investigating the dynamic behavior for a step-wise disturbance of +50 kJ kg^{-1} at $t = 100$ s in the enthalpy before economizer h_{bECO}. This value corresponds to a temperature change of approximately +11 °C at the nominal pressure. To demonstrate the performance of the two LQG controllers (EKF and KF-like LSO) for diverging time-constants, two simulations are presented, namely for constant $T_{\mathrm{full,O}} = 40$ s and $T_{\mathrm{full}} = \{40, 80\}$ s, just as in the Section before. $T_{\mathrm{full}} = 40$ s is thereby presented by the dashed-dotted lines, whereas $T_{\mathrm{full}} = 80$ s is depicted by the solid lines. As can be expected, performance becomes better,

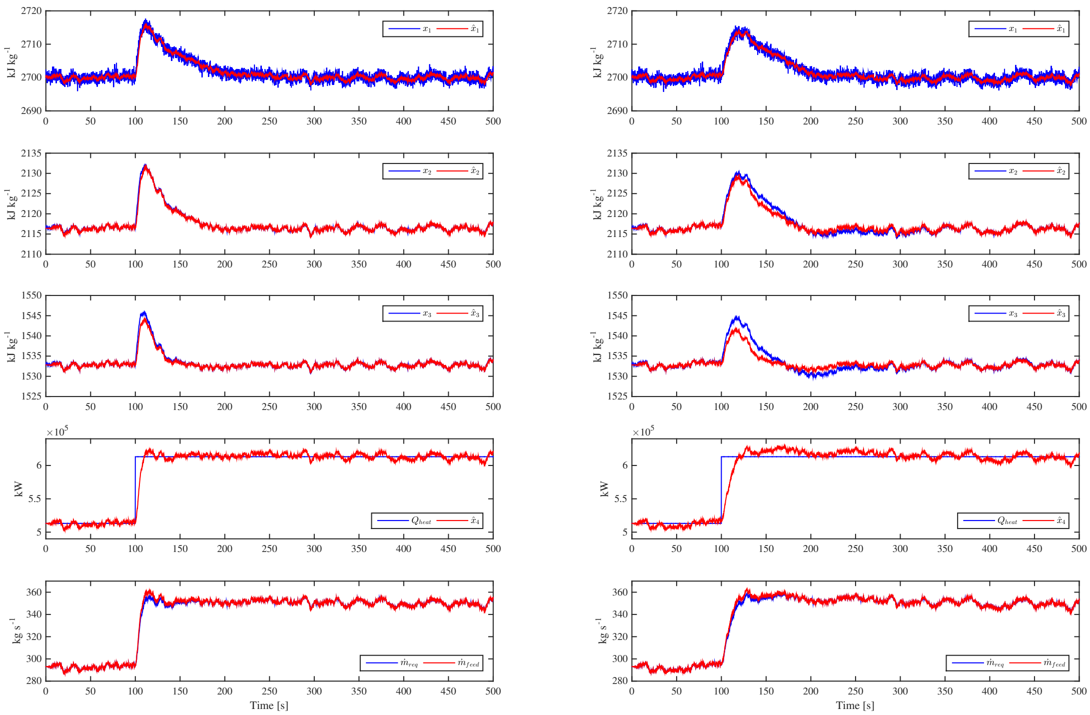

Figure 6: Standard EKF with noisy measurement of $h_{\text{aEVA,m}}$, disturbance in Q_{heat} and process noise. Left: $T_{\text{full}} = 40$ s, $T_{\text{full,O}} = 40$ s. Right: $T_{\text{full}} = 80$ s, $T_{\text{full,O}} = 40$ s.

the better the two time constant of the controller and the plant match. Like before, the two bottom plots show the feed water mass flow and the heat power, whereas the top three plots show the states x_i and their estimates $\hat{x}_i$, $i = 1, \ldots, 3$. While states x_2 and x_3 converge to new setpoints in order to compensate for the disturbance, the output h_{aEVA} is held at the nominal desired value h_{d}. Performance of the KF-like LSO on the right hand side is not much different compared to the EKF on the left hand side in this noise-free case.

5. Robustness investigation

In this Section, simulation results for the two different cases for robustness investigation as introduced in Section 3.5 are presented.

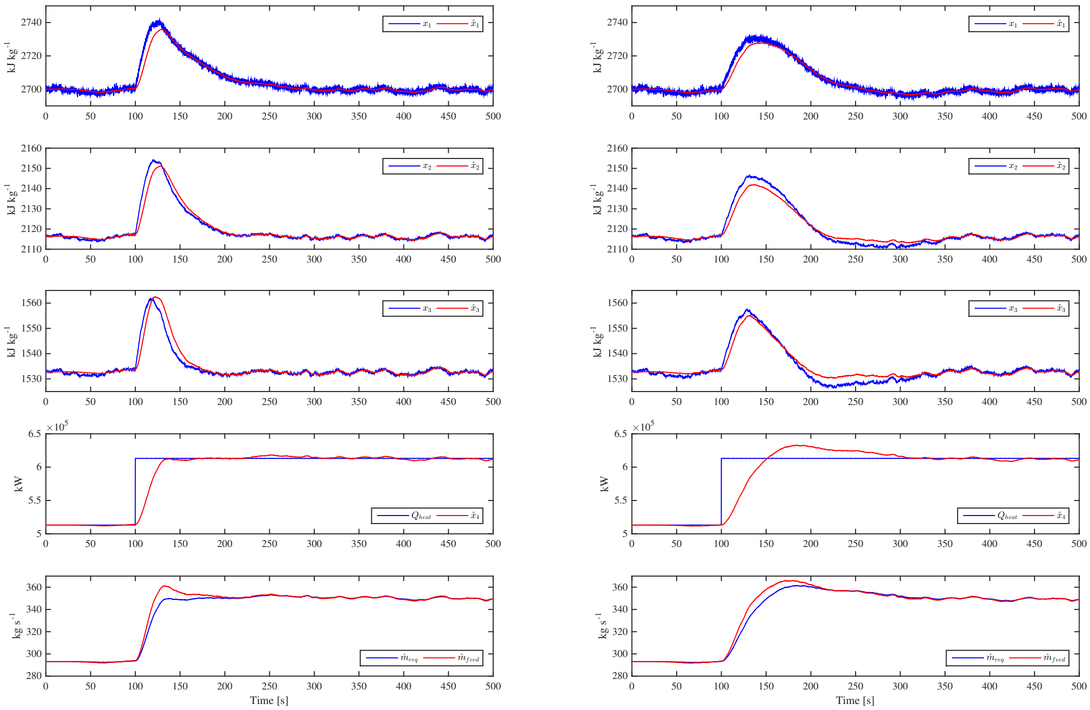

Figure 7: KF-like LSO with noisy measurement of $h_{\mathrm{aEVA,m}}$, disturbance in Q_{heat} and process noise. Left: $T_{\mathrm{full}} = 40$ s, $T_{\mathrm{full,O}} = 40$ s. Right: $T_{\mathrm{full}} = 80$ s, $T_{\mathrm{full,O}} = 40$ s.

5.1. Plant-model mismatch

In this simulation study a dynamic mismatch between the plant and the model is investigated. Thereby, the plant model is based on the sixth-order model (10), whereas the model in the LQG controller is still of third-order (7). In addition to the dynamic mismatch, several disturbances in the form of step changes and added white noises are implemented in the simulation, such that a high-fidelity model is the consequence:

- step change of $+50$ kJ kg^{-1} at $t = 100$ s for the enthalpy before economizer h_{bECO}
- step change of $+100$ MW at $t = 400$ s for Q_{heat}
- added white noise to the measurement $h_{\mathrm{aEVA,m}}$ with noise power 10^{-1}

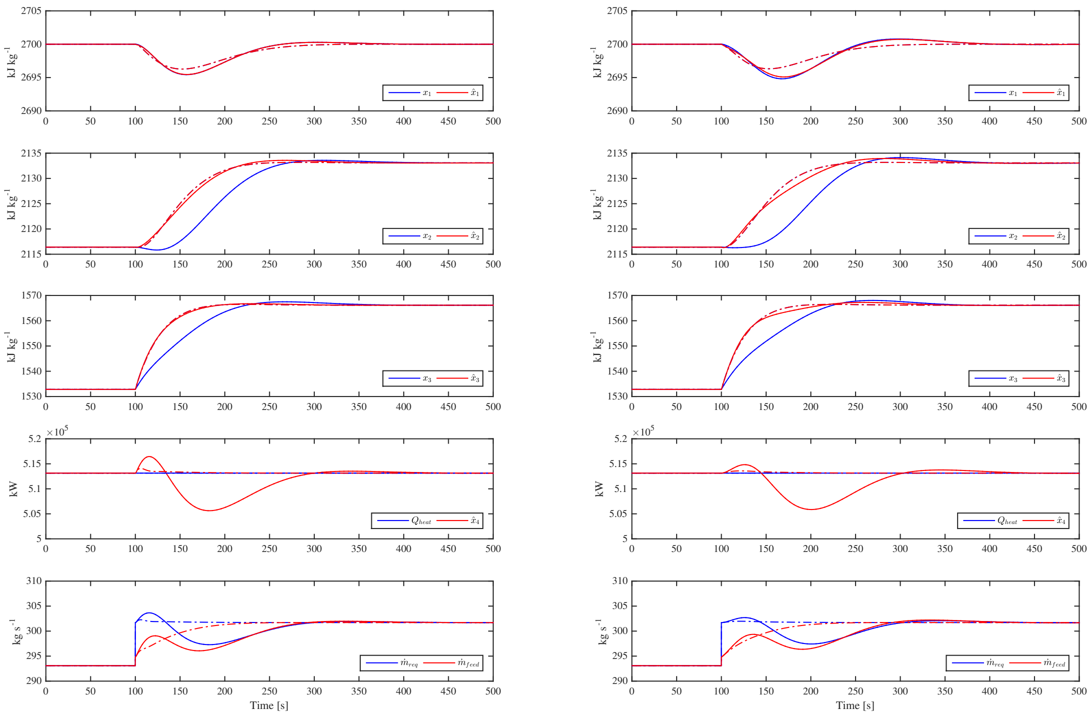

Figure 8: Simulation results for a disturbance in the enthalpy before economizer h_{bECO}. Left: EKF. Right: KF-like LSO

- added white noise to each state derivative in the sixth-order plant model with noise power 10^{-1} (process noise)

- added white noise to the enthalpy before economizer h_{bECO} with noise power 10^{0}

- added white noise to the heat value of the fuel H_{u} with noise power 10^{3}

The white noises listed above are implemented in Matlab Simulink as band-limited white noise processes making the results in this paper reproducible. Their sample time is 0.1 s and the chosen seed is [23341].

Two different simulations are presented, namely with matching time constants $T_{\mathrm{full,O}} = 40$ s and $T_{\mathrm{full}} = 40$ s in Figure 9 as well as different time constants $T_{\mathrm{full,O}} = 40$ s and $T_{\mathrm{full}} = 80$ s in Figure 10. Furthermore, the two observer designs (EKF and KF-like LSO) are compared. The arrangement of plots is the same as presented before, namely the three corresponding state-variables (compare Section 3.5) on the top three plots and the heat value as well as the feed water mass flow on the bottom plots, respectively. It can be seen that both LQG controllers (using EKF and KF-like LSO, respectively) are dealing well with all disturbances and the plant-model mismatch, meaning that the system can be stabilized even after introducing the step changes and noises. As before, the KF-like LSO has better noise suppression at the cost that convergence is slower compared to the EKF.

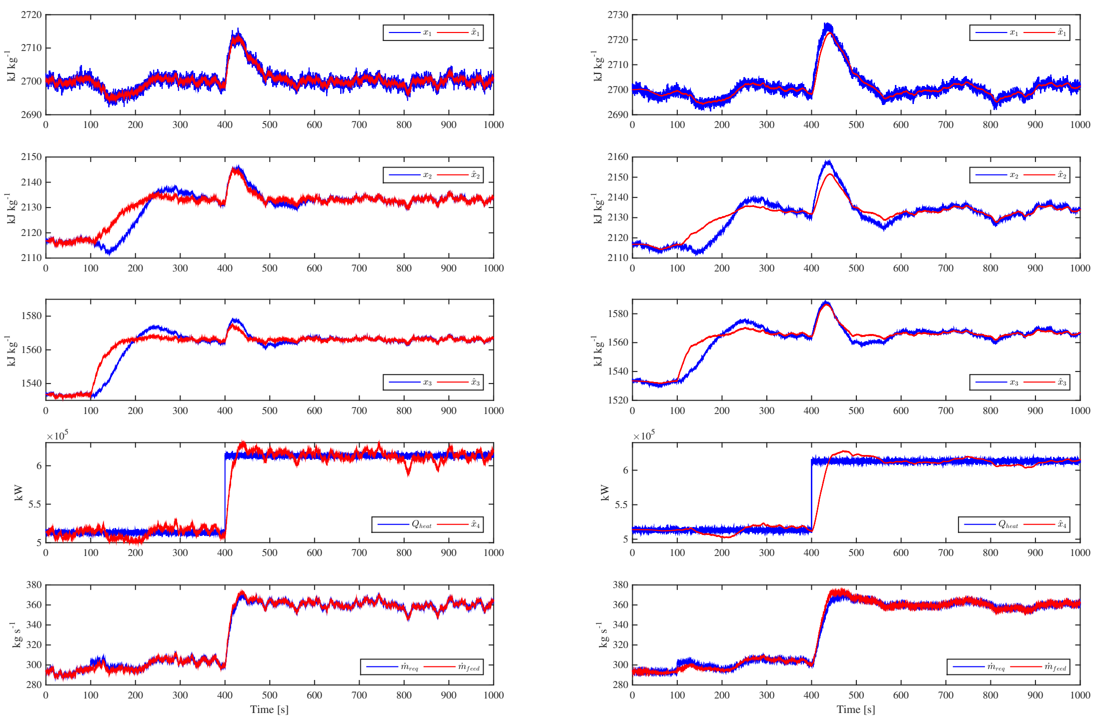

Figure 9: Plant-model-mismatch simulation with added noises for $T_{\text{full}} = 40$ s and $T_{\text{full,O}} = 40$ s. Left: EKF. Right: KF-like LSO

5.2. *Investigation of the damping ratio*

Here, the results of the robustness investigation based on the damping properties at full load are presented. The controller time constant is thereby held constant $T_{\text{full,O}} = 40$ s, whereas the plant's time constant varies $T_{\text{full,O}} = \{1, 5, 10, 20, 40, 80, 100, 150, 200, 250\}$ s. In addition, since the Jacobian of

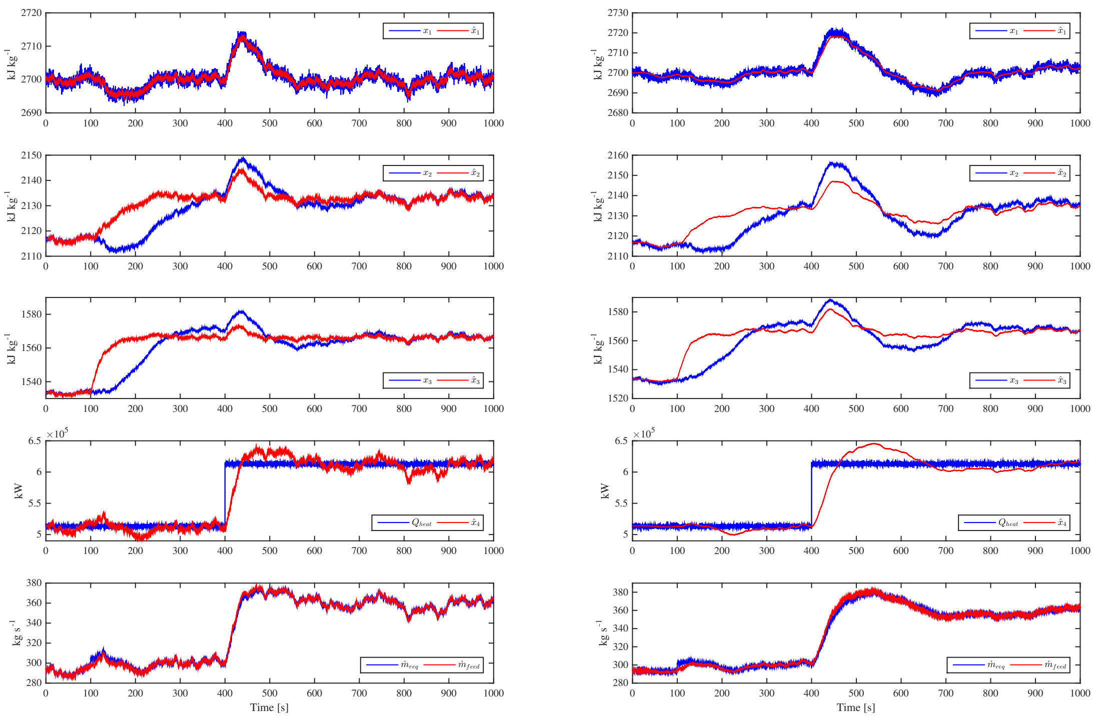

Figure 10: Plant-model-mismatch simulation with added noises for $T_{\text{full}} = 80$ s and $T_{\text{full,O}} = 40$ s. Left: EKF. Right: KF-like LSO

the LQG controller depends highly on the feed water mass flow, this is also varied from $1 - 500$ kg s^{-1}. The different colors in the plots represent results for different values of $q_{O,4}$, namely 10^5 (red), $5 \cdot 10^5$ (blue), 10^6 (black), $5 \cdot 10^6$ (green), 10^7 (magenta) and $5 \cdot 10^7$ (cyan). Furthermore, a constant line at a damping value of 0.3 is shown to represent the arbitrarily chosen minimal damping. As can be seen, the better the time constants of the plant and the controller match, the better the damping becomes, with only small dependency on the chosen value for $q_{O,4}$. It can be concluded that choosing small $q_{O,4}$ is beneficial if $T_{\text{full,O}}$ is larger than the real T_{full}, whereas larger $q_{O,4}$ seem the provide better damping properties if $T_{\text{full,O}}$ is smaller than T_{full}.

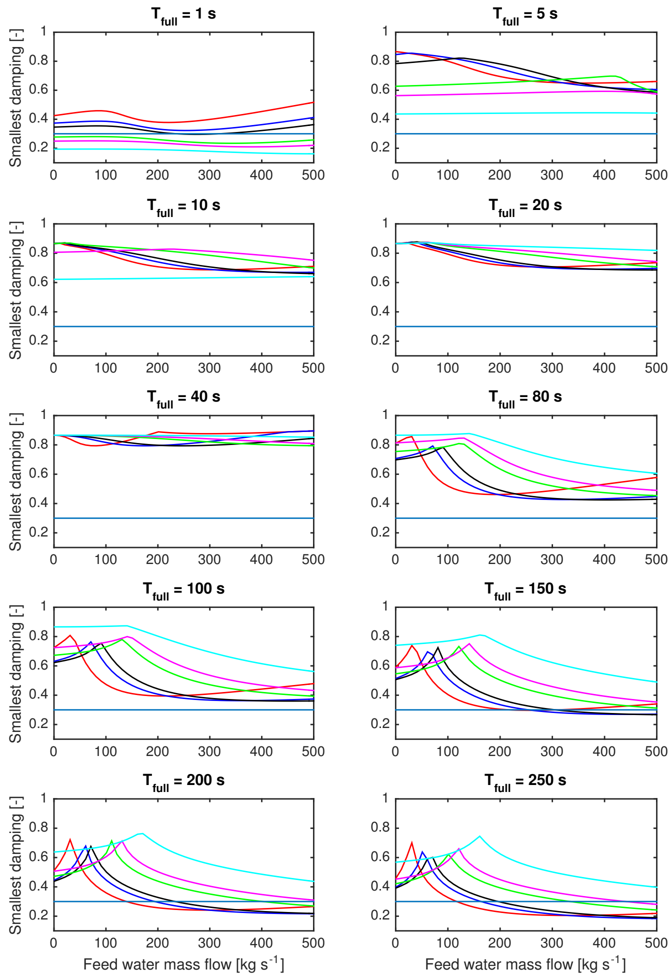

Figure 11: Damping properties as affected by different time constants, feed water mass flows and $q_{O,4}$

6. Conclusion

This work presented a novel approach for feed water supply control for an economizer-evaporator stage in a once-through boiler. The control objective was to deliver slightly superheated steam of constant quality after the evaporator. State-of-the-art controllers usually utilize temperature-cascades for this task, but in this work a state-controller based on an enthalpy model was used. The enthalpy-controller provided better and more accurate performance, whereas for temperature-cascade-controllers slight changes in pressure can cause unwanted occurrences of wet steam after the evaporator.

Two observer designs were presented and compared, namely a standard Extended Kalman Filter and a Kalman Filter-like least squares observer. The proposed LQG controllers showed good results regarding estimation and control performance. Since robustness is always an issue when designing LQG controllers, several disturbances and uncertainties were added to the plant model in order to demonstrate the robust nature of the controller.

Due to their simple tuning, the LQG controllers should be applied and tested on a real power plant. It should suffice to change the parameters $T_{\mathrm{full,O}}$ and $q_{O,4}$ or α, respectively, but also retuning of $\mathbf{Q_C}$, R_C and $\mathbf{Q_O}$ or α as well as R_{O} might be necessary in some cases.

Appendix: Simulation Parameters

Parameter	100 % load	70 % load	35 % load
H_{u} [kJ kg^{-1}]	26000	26000	26000
Q_{heat} [kW]	513240	387933	210210
T_{full} [s]	40	40	40
T_{sys} [s]	40	57.14	114.3
h_{bECO} [kJ kg^{-1}]	949.22	947.93	946.51
h_{d} [kJ kg^{-1}]	2700	2840	3000
$\dot{m}_{\mathrm{fuel}}$ [kg s^{-1}]	35	24.5	12.25
$\dot{m}_{\mathrm{feed,full}}$ [kg s^{-1}]	290	290	290
$\dot{m}_{\mathrm{req}}$ [kg s^{-1}]	290	203	101.5
p_{bECO} [bar]	200	163.1	120
p_{aEVA} [bar]	180	143.1	100
η [$-$]	0.564	0.609	0.66
$\vartheta_{\mathrm{bECO}}$ [°C]	220	220	220

LQG controller tunings:

$$
\begin{array}{lll}
\text{LQR:} & \mathbf{Q_C} = 10\,\mathbf{I}_3 & R_\mathrm{C} = 100, \\
\text{EKF:} & \mathbf{Q_O} = \begin{bmatrix} \mathbf{I}_3 & \mathbf{0}_{(3\times 1)} \\ \mathbf{0}_{(1\times 3)} & 5\cdot 10^7 \end{bmatrix}, & R_\mathrm{O} = 1, \\
\text{KF-like LSO:} & \alpha = 10^{-1}, & R_\mathrm{O} = 1,
\end{array}
$$

where $\mathbf{I}_n$ denotes an identity matrix of size n and $\mathbf{0}_{(m\times n)}$ indicates a marix of zeros with m rows and n columns.

References

[1] C. J. Backi, Entwurf und Test eines Zustandsreglers auf Basis des LQG-Verfahrens für die Enthalpieregelung eines Zwangdurchlaufkessels, Master's thesis, University of Stuttgart, Institute of Combustion and Power Plant Technology, this thesis is not publicly available due to patent claims of the Siemens AG (November 2009).

[2] C. J. Backi, M. Treuer, J. Gadinger, K. Wendelberger, B. Meerbeck, T. Weißbach, Method and Device for regulating the Production of Steam in a Steam Plant, Patent WO2011069700, Siemens AG, Germany (November 2011).

[3] C. J. Backi, Enthalpy control for the feed water supply in a once-through boiler with disturbance estimation, IFAC-PapersOnLine 50 (1) (2017) 1991–1996.

[4] L. Sun, D. Li, K. Y. Lee, Enhanced decentralized PI control for fluidized bed combustor via advanced disturbance observer, Control Engineering Practice 42 (2015) 128–139.

[5] K. Strauß, Kraftwerkstechnik, 6th Edition, Springer, 2009.

[6] M. Treuer, G. Scheffknecht, K. Wendelberger, B. Meerbeck, Neuer Ansatz zur Dampftemperaturregelung - genau, robust und leicht in Betrieb zu nehmen, in: Proceedings of the 41st Kraftwerkstechnisches Kolloquium, Dresden, Germany, 2009, pp. 509–519.

[7] J. W. Smith, Supercritical (Once Through) Boiler Technology, Tech. rep., Babcock & Wilcox Company, Ohio, USA (May 1998).

[8] J. Franke, R. Kral, Supercritical boiler technology for future market conditions, in: Proceedings of the 6th International Charles Parsons Turbine Conference, Dublin, Ireland, 2003.

[9] M. Klein, R. Kral, E. Wittchow, Benson boilers - experience in nearly 1000 plants and innovative design promise continuing success, Siemens Power Journal (1996) 26–30.

[10] G. Klefenz, Die Regelung von Dampfkraftwerken, 4th Edition, Bibliographisches Institut Wissenschaftsverlag, 1991.

[11] M. Rech, J. Rupp, K. Wendelberger, Innovative Control Strategies Improve Boiler Dynamic Response, Coal Power Magazine.

[12] E. Oko, M. Wang, Dynamic modelling, validation and analysis of coal-fired subcritical power plant, Fuel 135 (292–300).

[13] J.-Z. Liu, S. Yan, D.-L. Zeng, Y. Hu, Y. Lv, A dynamic model used for controller design of a coal fired once-through boiler-turbine unit, Energy 93 (2015) 2069–2078.

[14] H. Fan, Y.-F. Zhang, Z.-G. Su, B. Wang, A dynamic mathematical model of an ultra-supercritical coal fired once-through boiler-turbine unit, Applied Energy 189 (2017) 654–666.

[15] L. Sun, D. Li, K. Y. Lee, Y. Xue, Control-oriented modeling and analysis of direct energy balance in coal-fired boiler-turbine unit, Control Engineering Practice 55 (2016) 38–55.

[16] R. Starkloff, F. Alobaid, K. Karner, B. Epple, M. Schmitz, F. Boehm, Development and validation of a dynamic simulation model for a large coal-fired power plant, Applied Thermal Engineering 91 (2015) 496–506.

[17] K. Deng, C. Yang, H. Chen, N. Zhou, S. Huang, Start-Up and dynamic processes simulation of supercritical once-through boiler, Applied Thermal Engineering 115 (2017) 937–946.

[18] A. Sedić, S. Katulić, D. Pavković, Dynamic model of a natural water circulation boiler suitable for on-line monitoring of fossil/alternative fuel plants, Energy Conversion and Management 87 (2014) 1248–1260.

[19] L. Sun, Q. Hua, J. Shen, Y. Xue, D. Li, K. Y. Lee, Multi-objective optimization for advanced superheater steam temperature control in a 300 MW power plant, Applied Energy 208 (2017) 592–606.

[20] A. Weiss, I. Kolmanovsky, D. S. Bernstein, Forward-Integration Riccati-Based Output-Feedback Control of Linear Time-Varying Systems, in: Proceedings of the 2012 American Control Conference, Montréal, Canada, 2012, pp. 6708–6714.

[21] A. Prach, O. Tekinalp, D. S. Bernstein, A Numerical Comparison of Frozen-Time and Forward-Propagating Riccati Equations for Stabilization of Periodically Time-Varying Systems, in: Proceedings of the 2014 American Control Conference, Portland, Oregon, USA, 2014, pp. 5633–5638.

[22] R. M. Johnstone, C. R. Johnson, R. R. Bitmead, B. D. Anderson, Exponential convergence of recursive least squares with exponential forgetting factor, in: Proceedings of the 21st IEEE Conference on Decision and Control, Orlando, Florida, USA, 1982, pp. 994–997.

[23] H. Hammouri, J. De Leon Morales, Observer synthesis for state-affine systems, in: Proceedings of the 29th IEEE Conference on Decision and Control, Honululu, Hawaii, USA, 1990, pp. 784–785.

[24] M. A. M. Haring, Extremum-seeking control: convergence improvements and asymptotic stability, Ph.D. thesis, Norwegian University of Science and Technology (2016).